

Mild electropolymerization and monitoring of continuous film formation for
photoredox-active Ru metallopolymers

T. Schlotthauer,[‡] C. Friebe,[‡] A. M. Schwenke, M. Jäger
and U. S. Schubert**

Content

1	Experimental details.....	3
1.1	Instrumentation	3
1.2	Synthesis.....	3
1.3	Analytical characterization of complex II	4
2	Electropolymerization	5
2.1	Recovery and recycling studies of the complex.	8
3	Scanning electron microscopy	13
4	Electrochemical characterization of films	16
4.1	Cyclic voltammetry	16
5	Electrochemical impedance spectroscopy (EIS).....	20
5.1	Experimental data	20
5.2	Analysis of EIS data.....	22
6	UV-vis Characterization	24

1 Experimental details

1.1 Instrumentation

All electrochemical experiments were performed using a BioLogic VMP 3 potentiostat at room temperature under argon atmosphere. Cyclic voltammetry (CV) of solutions, containing ca. 10^{-4} M analyte and 0.1 M Bu_4NPF_6 in solvent that was stored under N_2 over molecular sieves, was carried out using a three-electrode setup with a glassy-carbon disk working electrode, a coiled platinum wire counter electrode, and a AgNO_3/Ag (CH_3CN) reference electrode. Electropolymerization experiments were executed using the same setup except for the working electrode, which was an ITO-coated glass slide (ca. $1 \times 3 \text{ cm}^2$, ca. 1 cm^2 submerged in the solution). CV measurements were conducted utilizing polymer-coated ITO/glass slides as working electrode. Surface-coverage values were calculated *via* determination of the area under the baseline-corrected CV curves recorded at scan rates of 5, 20, and $50 \text{ mV}\cdot\text{s}^{-1}$ yielding the electrical charge that can be collected by the film Q . The obtained charge value was converted to the surface coverage using the macroscopic film area A and assuming that two one-electron redox processes ($\text{Ru}^{\text{III}}/\text{Ru}^{\text{II}}$ and quaterthiophene $^{+/0}$) are involved in the voltammetric signal *via* $\Gamma = \frac{Q}{2FA}$.

Electrochemical impedance spectroscopy (EIS) was carried out using the same setup as for CV. The EIS measurements were executed potentiostatically; different dc potentials were applied and ac frequencies from 1 MHz to 10 mHz and an ac voltage amplitude of 10 mV were used.

UV-vis measurements of solutions and films were performed on a PerkinElmer LAMBDA 750 UV/Vis/NIR Spectrophotometer. UV-vis emission measurements of solutions and films were conducted using a Jasco FP6500 spectrometer and a Tecan infinite M200 Pro microplate reader, respectively. Solutions contained ca. 10^{-6} M analyte in spectrophotometric-grade solvent and were measured using 1-cm quartz cuvettes. Films were measured deposited onto ITO-coated glass slides.

UV-vis-NIR spectroelectrochemistry was conducted on a PerkinElmer LAMBDA 750 UV-vis-NIR Spectrophotometer in combination with a BioLogic VMP 3 potentiostat using the polymer-coated ITO/glass slides as working electrode, a platinum-rod counter electrode, and a AgNO_3/Ag (CH_3CN) reference electrode.

Surface topography and film thicknesses were measured using an optical interferometric profiler Wyko NT9100 (Veeco, Germany). The instrument is equipped with three objectives (2.5 \times , 5 \times , and 20 \times), which enable effective magnifications between 1 \times to 40 \times .

Scanning electron microscopy images were acquired with a field-emission SEM Sigma VP (Carl Zeiss) with *in-lense* or backscattering electron detector. Prior to the measurement, the samples were coated with a thin layer of carbon. Cross-sections were prepared by scratching the backside of the glass supports with a diamond knife and thereafter manually breaking the slide.

1.2 Synthesis

Complex II. A microwave vial was charged with $[\text{Ru}(\text{dqp})(\text{dqp}(\text{PhBr})_2)](\text{PF}_6)_2$ (50 mg, 0.037 mmol), 2,2-bithiophene-5-boronic acid pinacol ester (42.8 mg, 0.146 mmol), $\text{Pd}(\text{dba})_2$ (1.26 mg, 2.2 μmol), SPHOS (2.7 mg, 6.58 μmol), and K_2CO_3 (30.3 mg, 0.219 mmol), dissolved in 1.5 mL CH_3CN and 0.75 mL H_2O . The solution was deaerated with N_2 for 10 min and heated for 16 h at 100 $^\circ\text{C}$. Afterwards, the reaction mixture was cooled to room temperature and precipitated in aqueous NH_4PF_6 solution. The aqueous solution was extracted three times with CH_2Cl_2 and the combined organic layers were washed with water and brine. The mixture was dried over Na_2SO_4 , filtered, and the solvent was evaporated under reduced pressure. The crude product was purified *via* flash column chromatography using amino-functionalized silica and a mixture of CH_2Cl_2 and CH_3CN (98:2) as

eluent. Final purification was done by diffusion-controlled crystallization with CH₃CN and diethyl ether to obtain 12 mg (21%) of the pure complex. ¹H NMR (600 MHz, CD₃CN) δ 8.21 (td, *J* = 8.0, 6.1 Hz, 2H), 8.15 (d, *J* = 5.3 Hz, 2H), 8.13 (dd, *J* = 5.2, 1.3 Hz, 2H), 8.09 (dd, *J* = 8.1, 1.2 Hz, 2H), 7.99 – 7.94 (m, 2H), 7.92 (d, *J* = 8.0 Hz, 4H), 7.90 (d, *J* = 8.3 Hz, 4H), 7.75 (dd, *J* = 9.8, 8.0 Hz, 4H), 7.70 (d, *J* = 7.4 Hz, 2H), 7.55 (dd, *J* = 5.9, 2.0 Hz, 6H), 7.52 – 7.48 (m, 2H), 7.44 (dd, *J* = 8.4, 7.4 Hz, 2H), 7.42 (dd, *J* = 5.1, 1.0 Hz, 2H), 7.36 (dd, *J* = 3.5, 1.0 Hz, 2H), 7.34 (d, *J* = 3.7 Hz, 2H), 7.12 (dd, *J* = 5.1, 3.6 Hz, 2H), 7.10 (dd, *J* = 8.1, 5.2 Hz, 2H), 7.06 (d, *J* = 5.4 Hz, 2H) ppm. ¹³C NMR (151 MHz, CD₃CN) δ 180.7, 159.5, 158.7, 157.9, 157.7, 149.9, 148.0, 147.8, 142.4, 141.1, 139.3, 138.7, 138.6, 137.6, 136.2, 135.8, 134.1, 133.9, 133.2, 133.1, 131.8, 131.6, 129.4, 129.3, 129.2, 127.9, 127.8, 126.7, 126.5, 126.4, 126.2, 125.9, 125.3, 123.2, 123.1 ppm. HRMS (ESI) *m/z*: [M - 2(PF₆)]²⁺ calcd for C₇₄H₄₆N₆RuS₄, 624.0850; found: 624.0858; Error: 0.9 ppm. UV-vis (CH₃CN): λ_{max} (ε) = 503 (22400), 376s (55700), 354 (58700), 287 nm (34400); Emission (CH₃CN): λ_{max} = 744 nm.

1.3 Analytical characterization of complex II

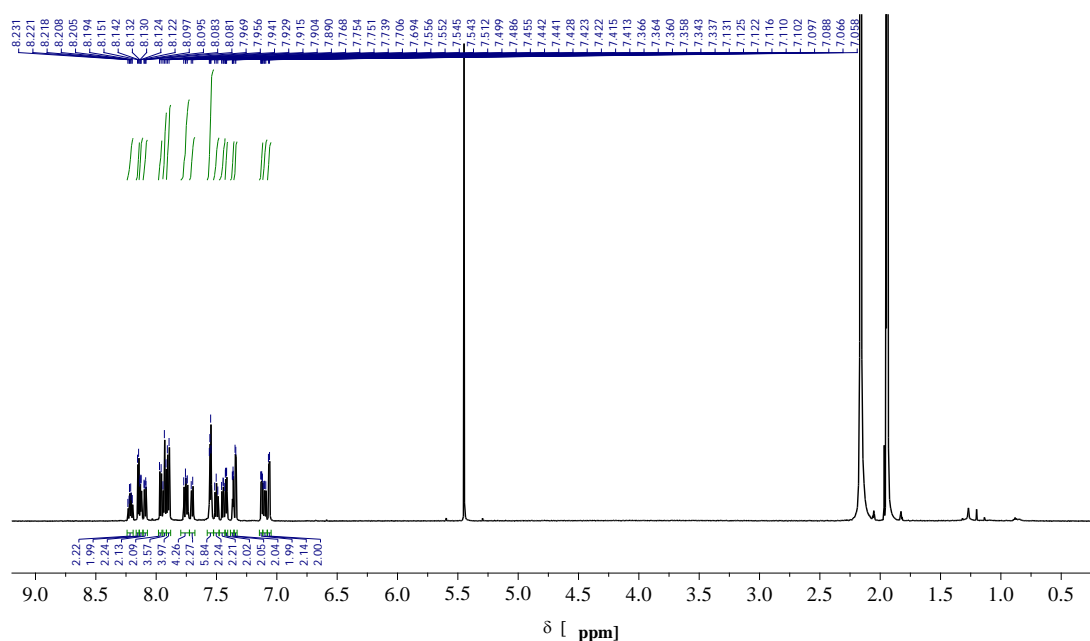


Fig. S1. ¹H NMR spectrum (600 MHz, CD₃CN) of **complex II**.

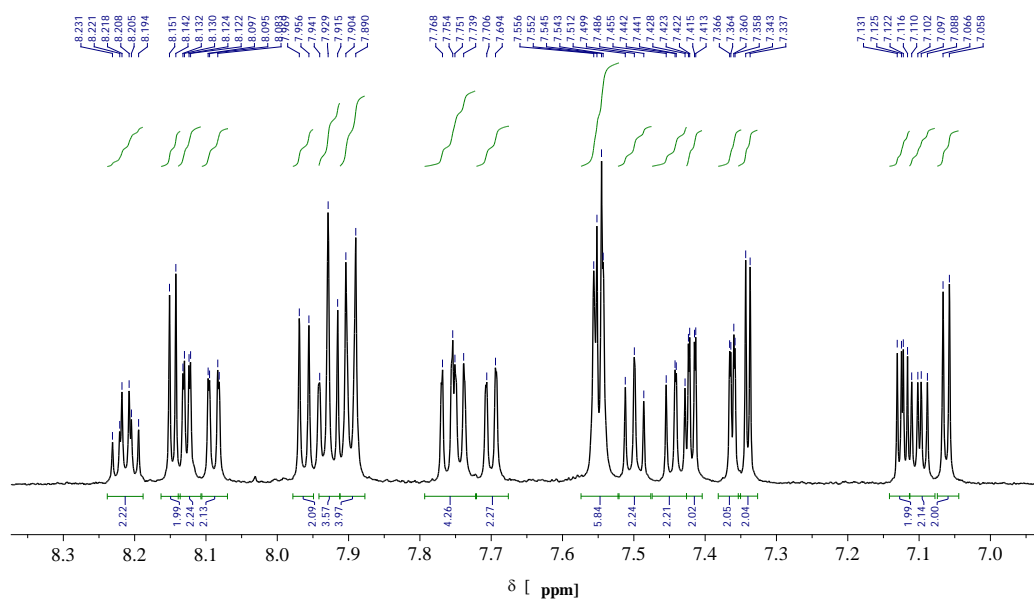


Fig. S2. ¹H NMR spectrum (600 MHz, CD₃CN, aromatic region) of **complex II**.

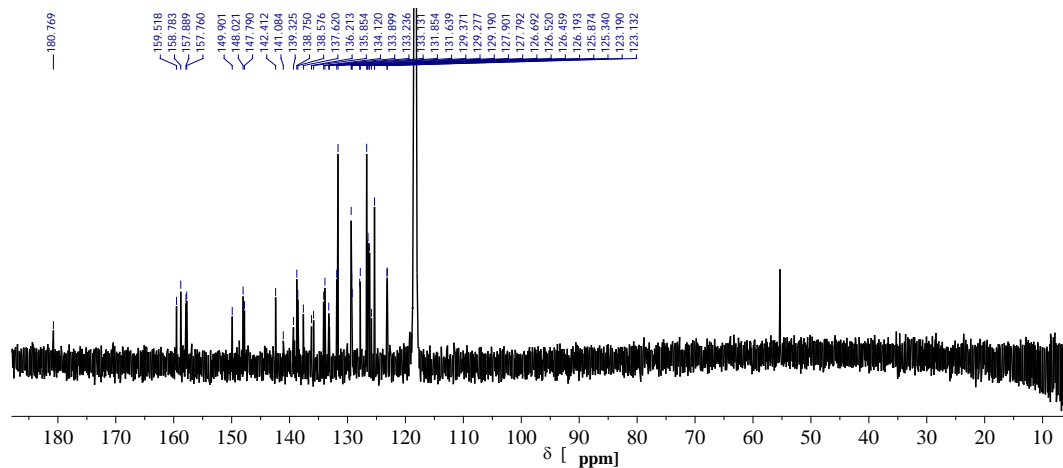


Fig. S3. ^{13}C NMR spectrum (151 MHz, CD_3CN) of **complex II**.

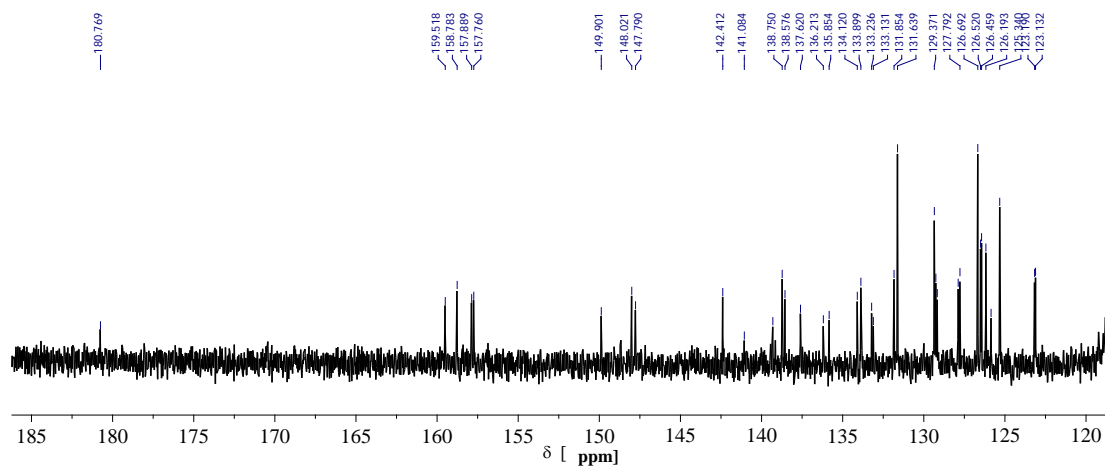


Fig. S4. ^{13}C NMR spectrum (151 MHz, CD_3CN , aromatic region) of **complex II**.

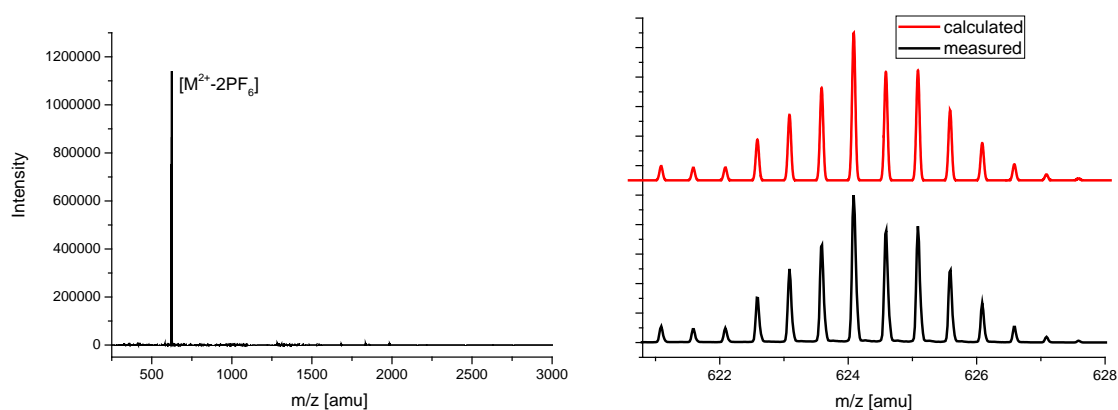


Fig. S5. High-resolution ESI-ToF mass spectrum of **complex II** and isotope simulation.

2 Electropolymerization

All voltammograms are given *vs.* AgNO_3/Ag . Ferrocene was added as an internal reference; the redox potential of the Fc^+/Fc couple was found at approximately +0.094 V *vs.* AgNO_3/Ag .

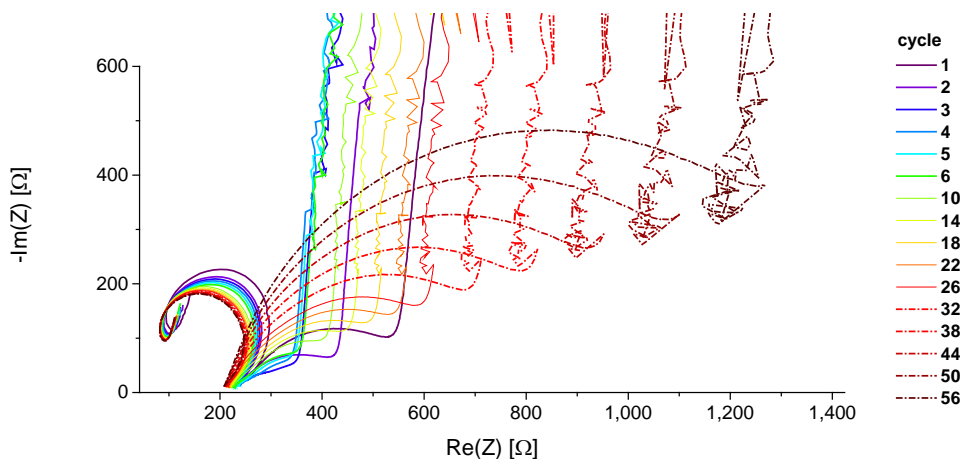


Fig. S6. Electrochemical impedance spectra of **p1** (at 0.7 V vs. AgNO₃/Ag) over the course of the potentiodynamic electropolymerization of complex **I** on glassy carbon in the presence of BFEE (200 mV·s⁻¹, 0.1 M Bu₄NPF₆ in CH₃CN, 5vol% BFEE) taken after every cycle (black), every third cycle (red) and every fifth cycle (blue). Arrow indicates begin of characteristic half-cycle assigned to film resistance (decreasing frequencies evolve from left to right), showing the typical semi-circle starting at 200 Ω after 10 cycles. See Section 5.2 for more details.

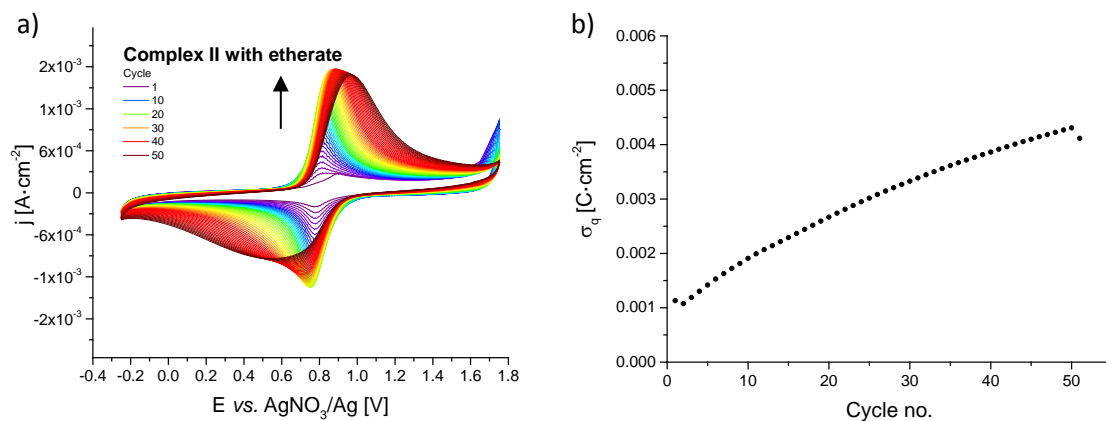


Fig. S7. (a) Development of the CV and (b) development of the cathodic charge obtained for **p2** from the CV over the course of potentiodynamic electropolymerization of complex **II** on glassy carbon in the presence of BFEE (-0.25 to 1.75 V vs. AgNO₃/Ag, 200 mV·s⁻¹, 50 cycles; 0.1 M Bu₄NPF₆ in CH₃CN, 5vol% BFEE).

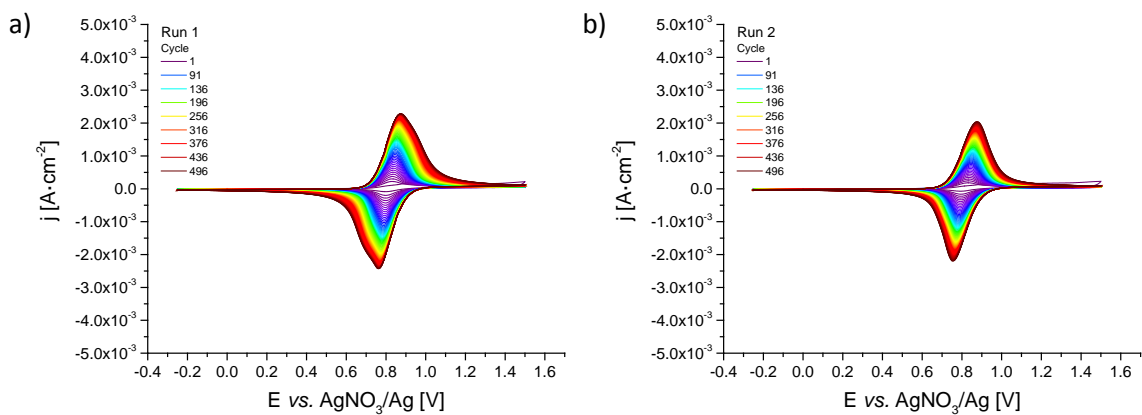


Fig. S8. Development of the CV over the course of potentiodynamic electropolymerization (-0.25 to 1.5 V vs. AgNO_3/Ag , $200 \text{ mV}\cdot\text{s}^{-1}$, 500 cycles; $0.1 \text{ M Bu}_4\text{NPF}_6$ in CH_3CN with $1 \text{ mol}\%$ H_2O) from (a) a fresh solution (**p5a**) and (b) second attempt from the same solution (**p5b**).

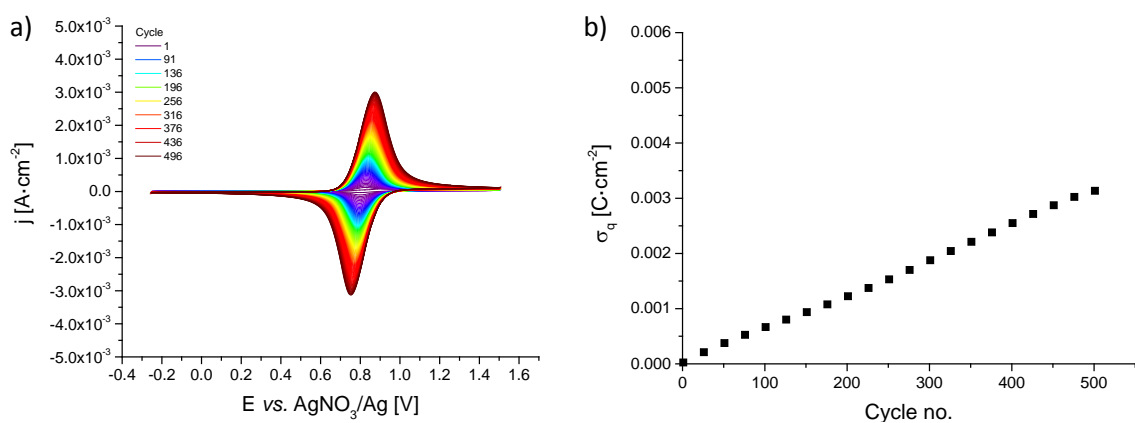
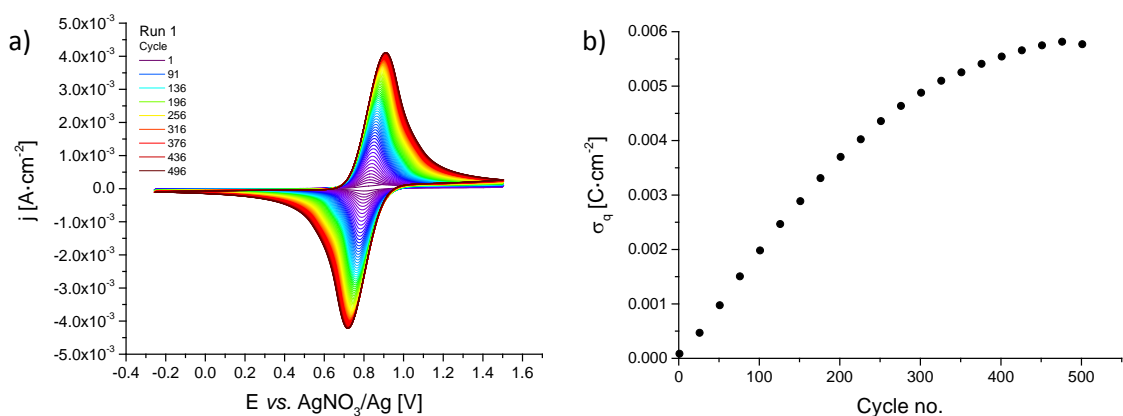


Fig. S9. (a) Development of the CV and (b) development of the cathodic charge over the course of potentiodynamic electropolymerization of **p6** (-0.25 to 1.5 V vs. AgNO_3/Ag , $200 \text{ mV}\cdot\text{s}^{-1}$, 500 cycles; $0.1 \text{ M Bu}_4\text{NPF}_6$ in CH_3CN with $3 \times 10^{-4} \text{ M HPF}_6$).



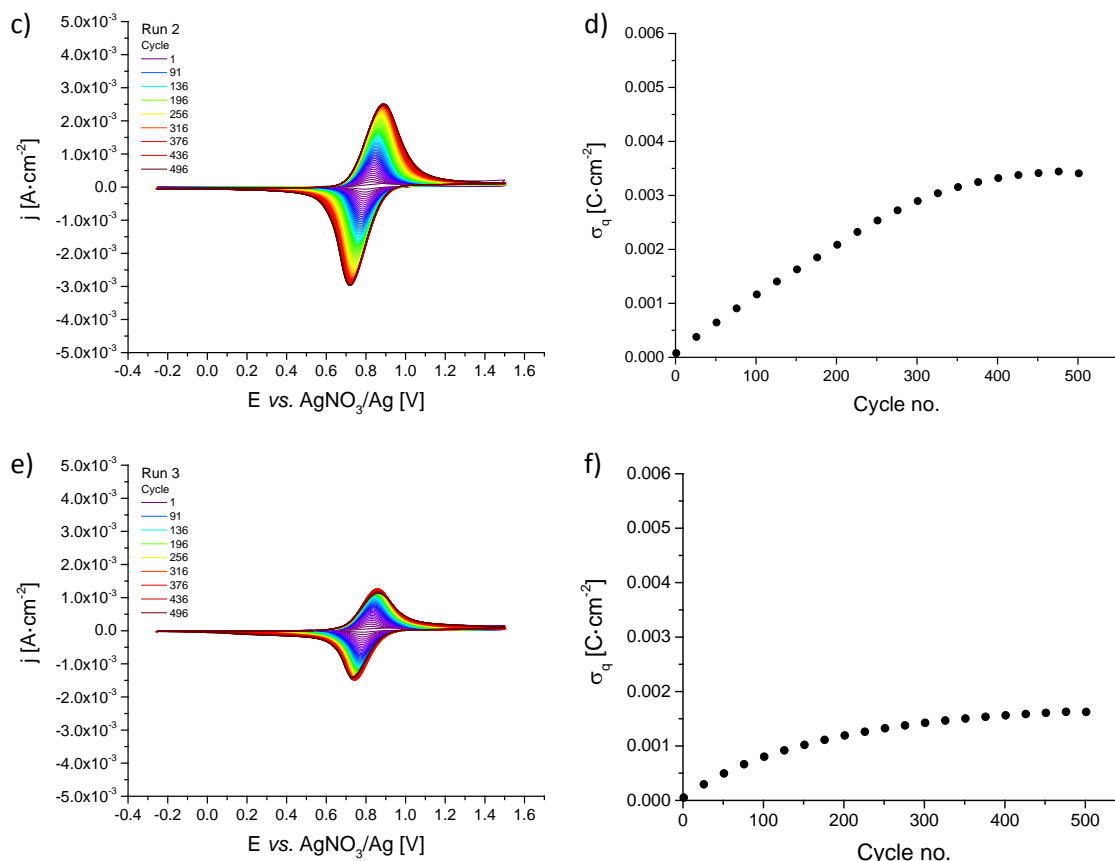


Fig. S10. Development of the CV (a, c, e) and development of the cathodic charge obtained from the CV (b,d,f) over the course of potentiodynamic electropolymerization (-0.25 to 1.5 V vs. AgNO₃/Ag, 200 mV·s⁻¹, 500 cycles; 0.1 M Bu₄NPF₆ in CH₃CN): (a, b) **p7a** using fresh solution, (c, d) **p7b** by immersing a fresh electrode using the remaining solution from **p7a**, and (e, f) **p7c** by immersing a fresh electrode using the remaining solution of **p7b**.

2.1 Recovery and recycling studies of the complex.

The solutions from various electropolymerization experiments were combined (an aliquot was kept for later comparison) and the complex was recovered. After removal of excess of solvent under reduced pressure, the solids were dissolved in hot methanol. Upon cooling and standing at room temperature, an excess of TBAPF₆ crystallized and was removed by filtration. The filtrate was collected, and excess of solvent was removed under reduced pressure. ¹H NMR analysis, ESI-ToF MS and UV-vis absorption of the recovered batch showed slight differences to the pristine complex (Fig. S11 and Fig. S12).

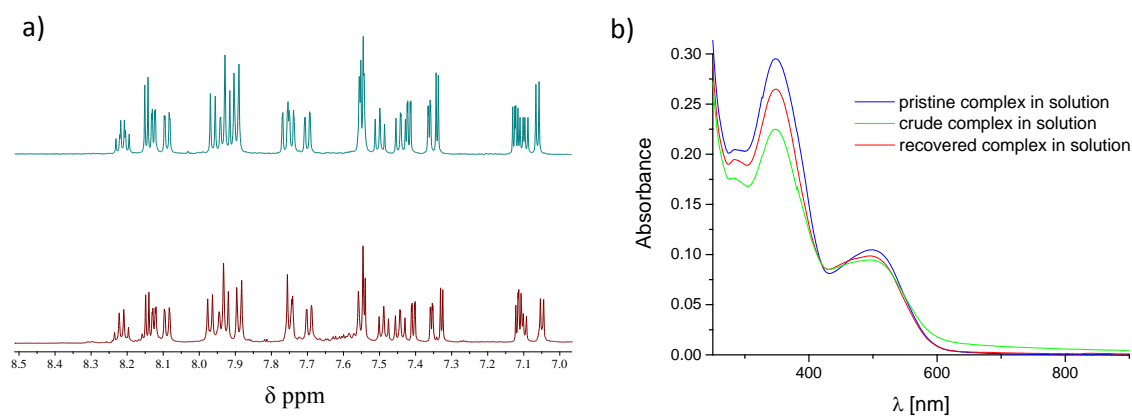


Fig. S11. (a) ¹H NMR spectra of the pristine complex (top) and the recovered complex (bottom), and (b) UV-vis absorption spectra taken in electrolyte solution (CH₃CN, 0.1 M TBAPF₆).

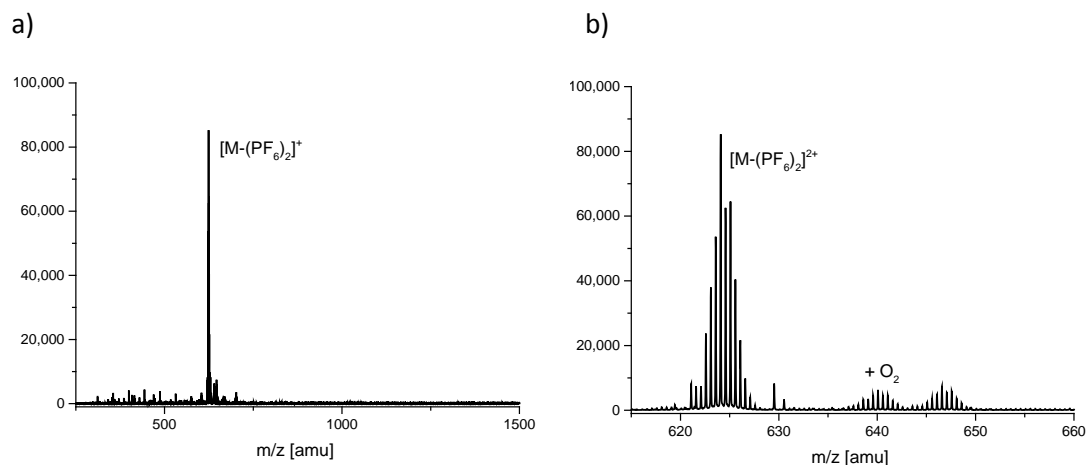


Fig. S12. (a) Full ESI-ToF MS after purification, and (b) enlargement to illustrate occurrence of multiple-oxygenated Ru side products.

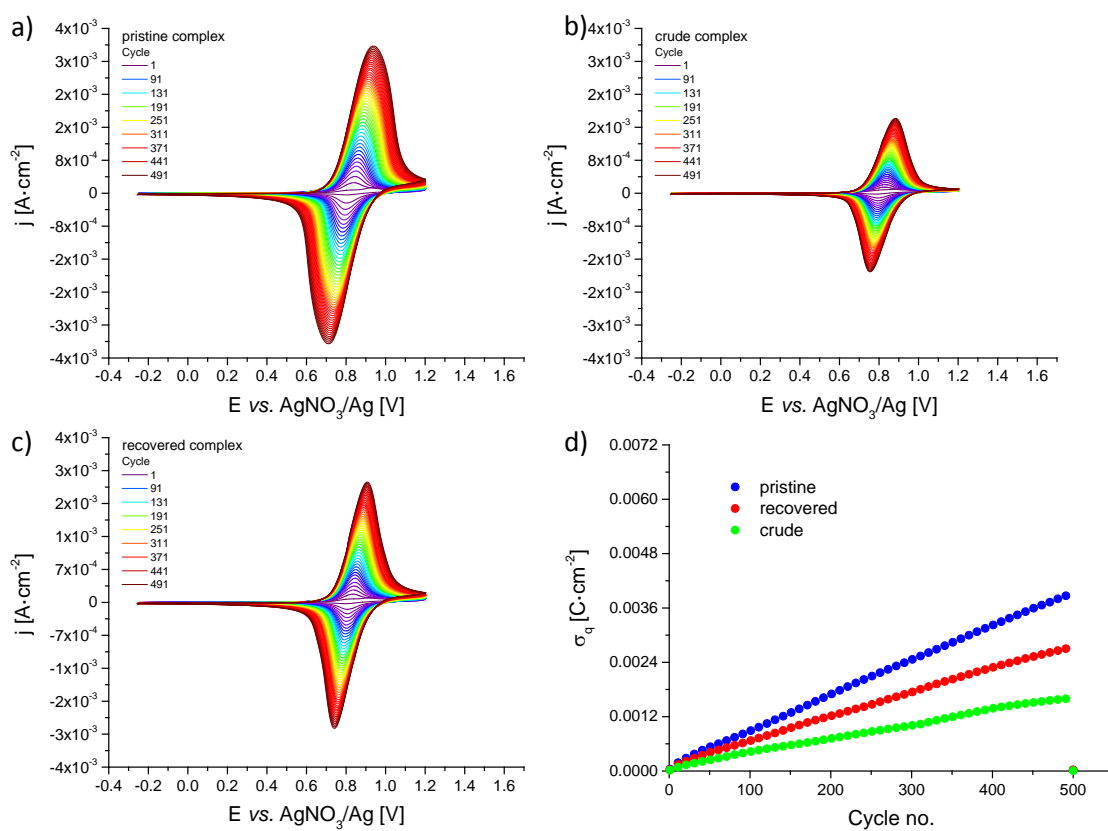


Fig. S13. Development of the CV of (a) the pristine complex (**p8a**), (b) the crude complex without purification (**p8b**), and (c) the purified complex (**p8c**). (d) Development of the cathodic charge over the course of potentiodynamic electropolymerization (-0.25 to 1.2 V vs. AgNO₃/Ag, 200 mV·s⁻¹, 500 cycles; 0.1 M Bu₄NPF₄ in CH₃CN).

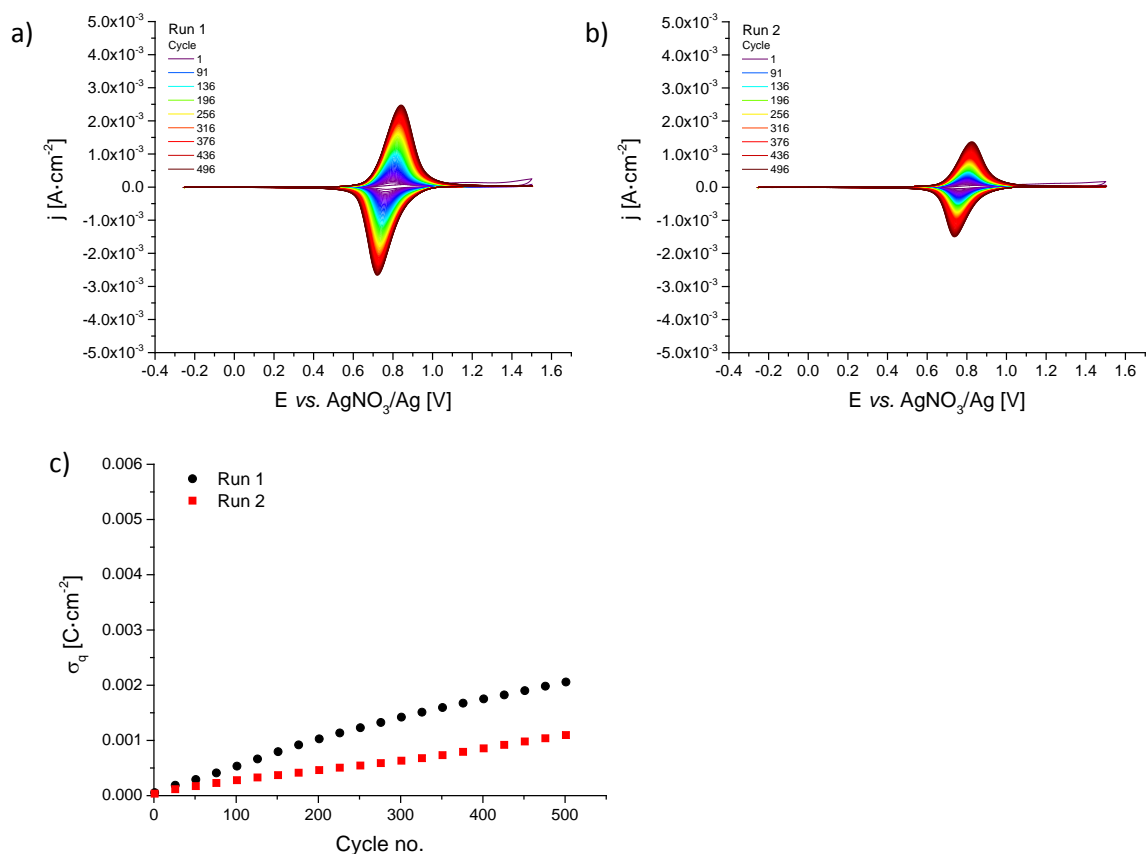


Fig. S14. Development of the CV over the course of potentiodynamic electropolymerization (-0.25 to 1.5 V vs. $AgNO_3/Ag$, 200 $mV \cdot s^{-1}$, 500 cycles; 0.1 M Bu_4NClO_4 in CH_3CN) from (a) a fresh solution (**p9a**) and (b) second attempt from the same solution (**p9b**); (c) development of the cathodic charge.

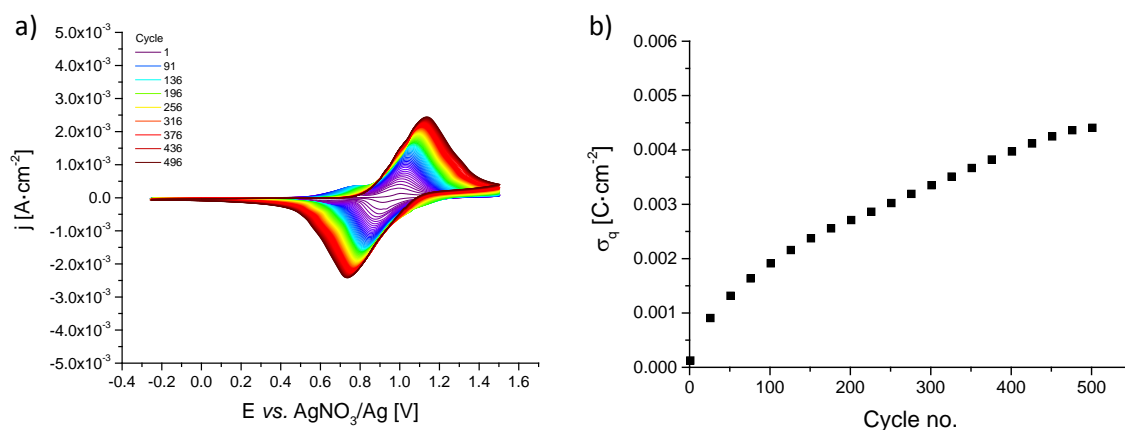


Fig. S15. (a) Development of the CV and (b) development of the cathodic charge over the course of potentiodynamic electropolymerization of **p10** (-0.25 to 1.5 V vs. $AgNO_3/Ag$, 200 $mV \cdot s^{-1}$, 500 cycles; 0.1 M Bu_4NPF_6 in CH_2Cl_2).

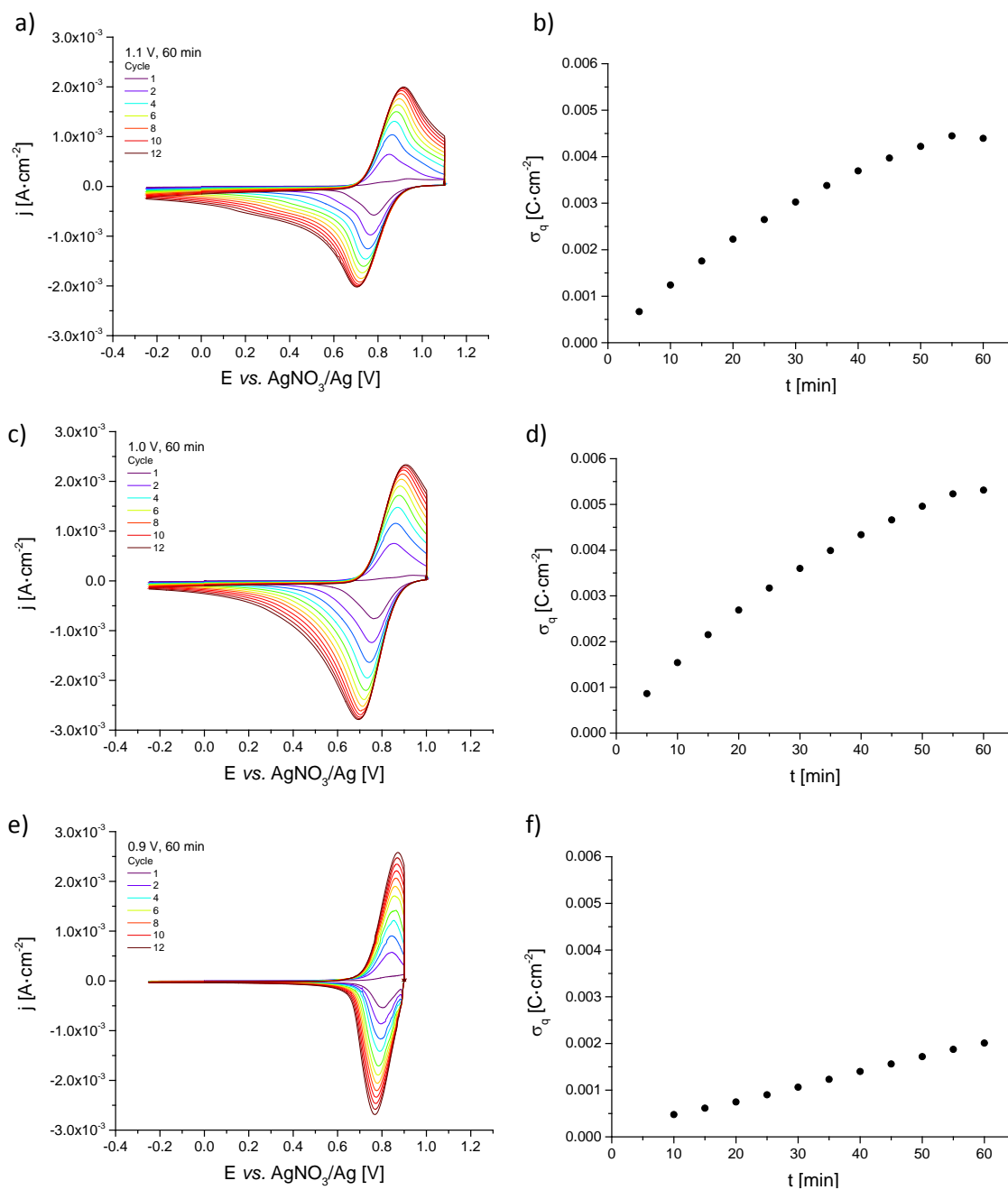


Fig. S16. Development of the CV (a, c, e) and development of the cathodic charge (b, d, f) over the course of potentiostatic electropolymerization (potentials vs. AgNO₃/Ag, hold time 60 min; 0.1 M Bu₄NPF₆ in CH₃CN; CV measured after every 5 min); hold potentials: (a) **p11** at 1.1 V, (c) **p12** at 1.0 V, and (e) **p13** at 0.9 V.

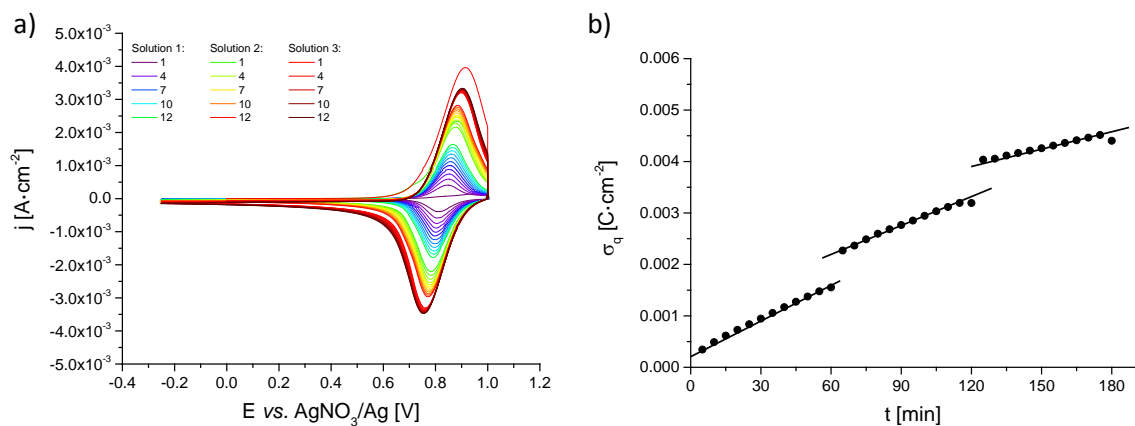


Fig. S17. (a) Development of the CV and (b) development of the cathodic charge over the course of potentiostatic electropolymerization (1.0 V vs. AgNO_3/Ag , 3×60 min; 0.1 M Bu_4NPF_6 in CH_3CN ; CV measured after every 5 min). After every 60 min, the solution was replaced with fresh solution (**p14a-c**).

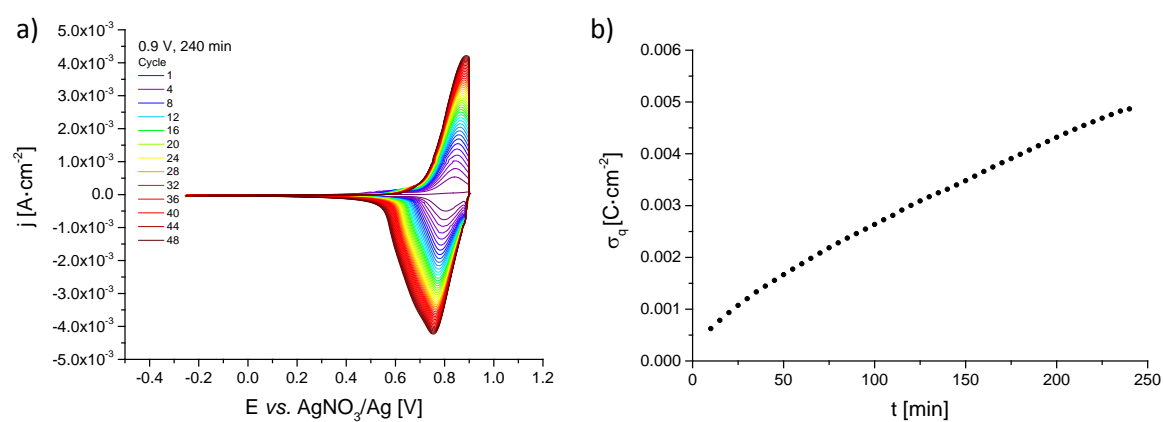


Fig. S18. (a) Development of the CV and (b) development of the cathodic charge over the course of potentiostatic electropolymerization of **p15** (0.9 V vs. AgNO_3/Ag , 240 min; 0.1 M Bu_4NPF_6 in CH_3CN ; CV measured after every 5 min).

3 Scanning electron microscopy

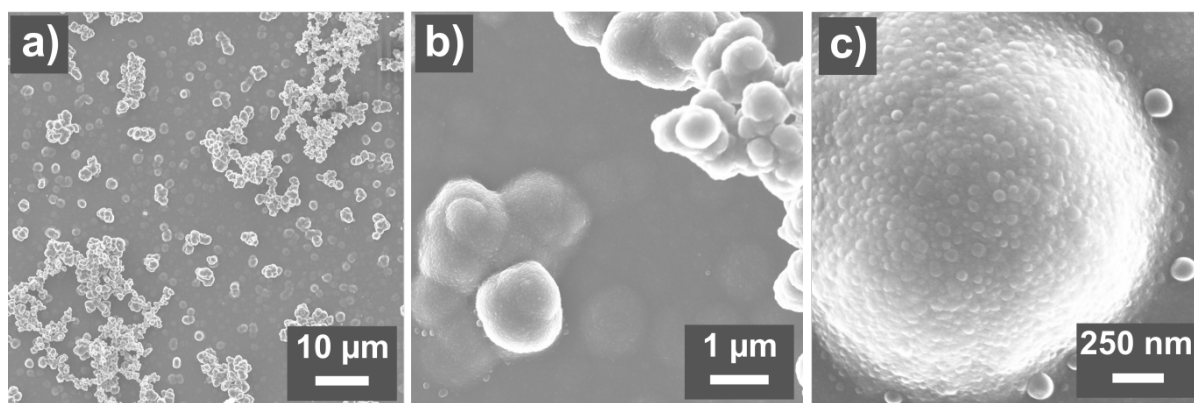


Fig. S19. SEM images at different magnifications of potentiodynamically prepared film **p5a** (−0.25 to 1.5 V vs. AgNO₃/Ag, 200 mV·s^{−1}, 500 cycles; 0.1 M Bu₄NPF₆ in CH₃CN with 1m% H₂O).

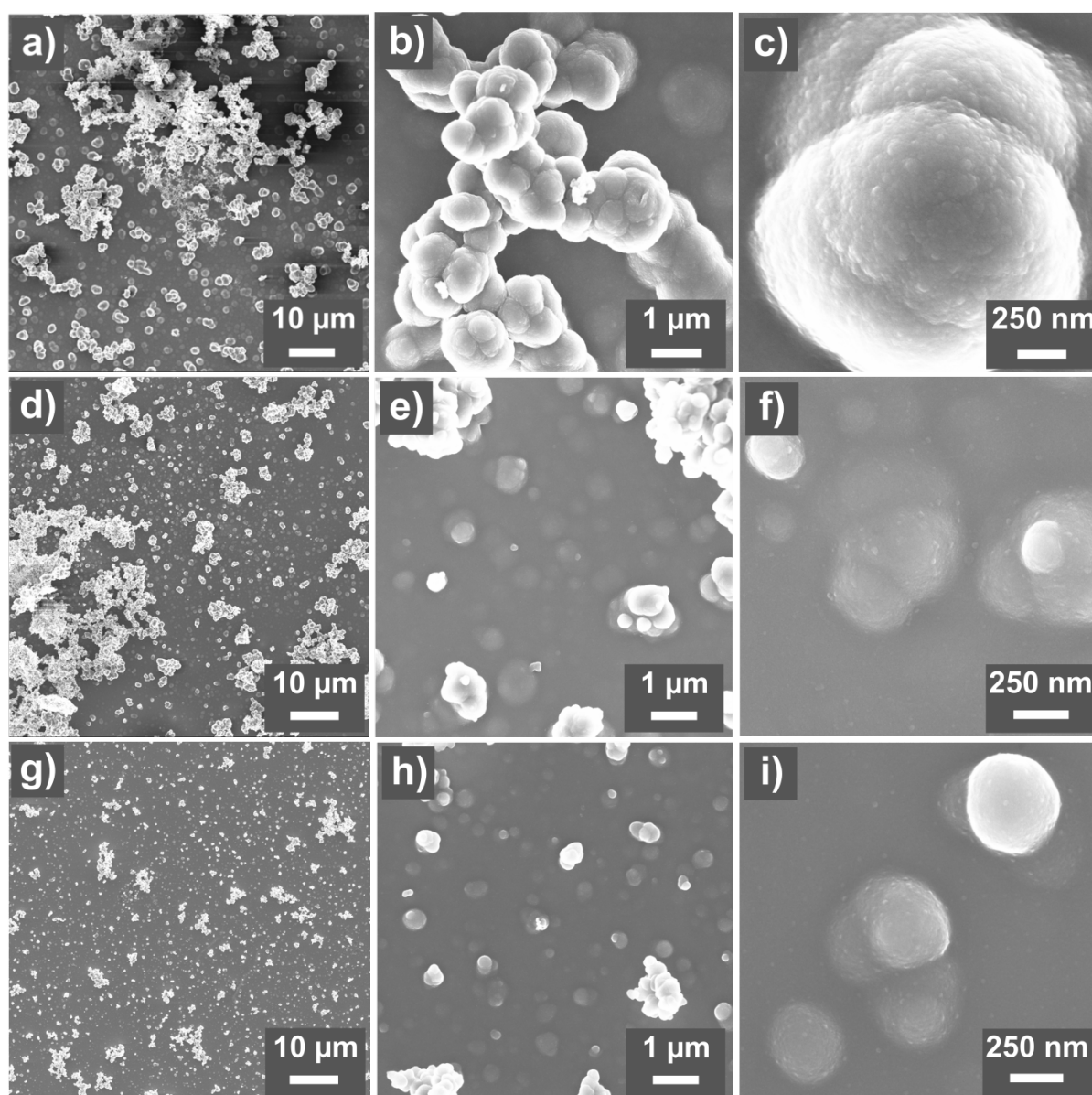


Fig. S20. SEM images at different magnifications of potentiodynamically prepared films (−0.25 to 1.5 V vs. AgNO₃/Ag, 200 mV·s^{−1}, 500 cycles; 0.1 M Bu₄NPF₆ in CH₃CN) consecutively obtained from the same solution (**p7a** (a–c), **p7b** (d–f), and **p7c** (g–i) corresponding to the fresh solution, second, and third attempt, respectively).

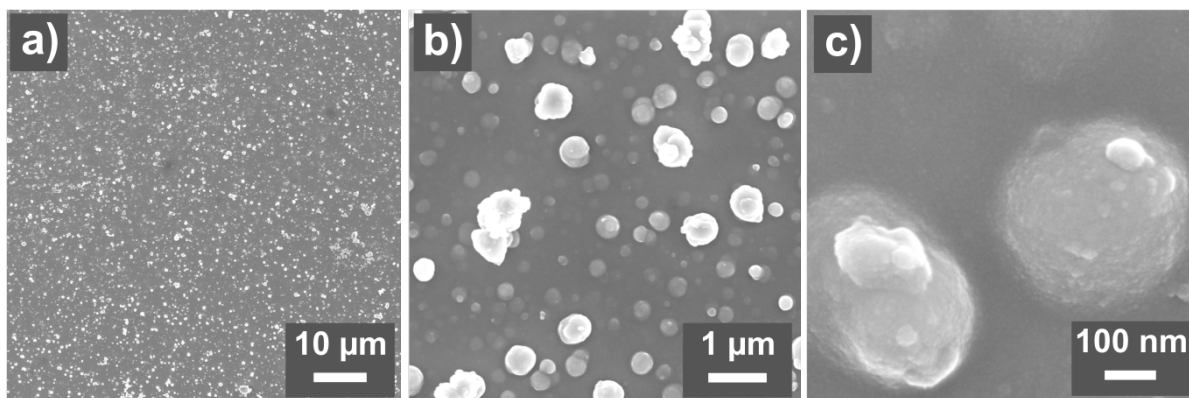


Fig. S21. SEM images at different magnifications of a potentiodynamically prepared film **p9a** (−0.25 to 1.5 V vs. AgNO₃/Ag, 200 mV·s^{−1}, 500 cycles; 0.1 M Bu₄NClO₄ in CH₃CN).

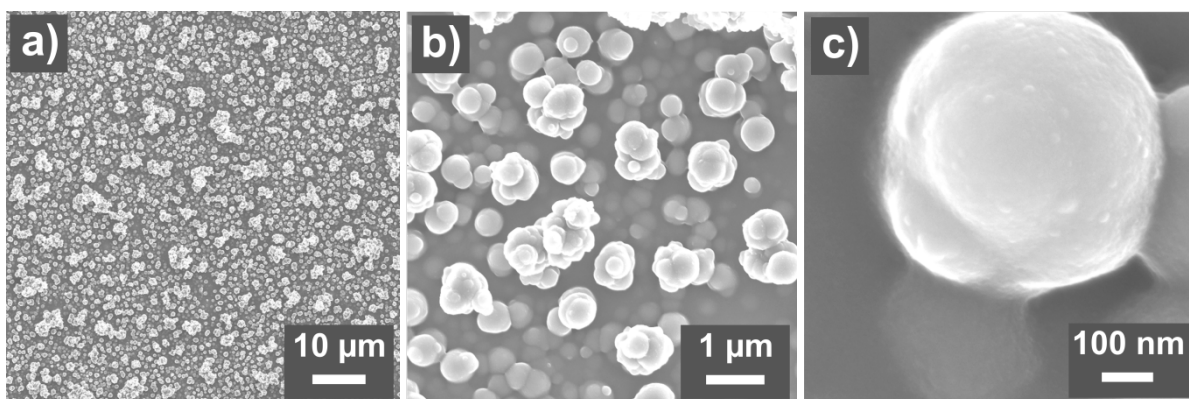


Fig. S22. SEM images at different magnifications of potentiodynamically prepared film **p10** (−0.25 to 1.5 V vs. AgNO₃/Ag, 200 mV·s^{−1}, 500 cycles; 0.1 M Bu₄NPF₆ in CH₂Cl₂).

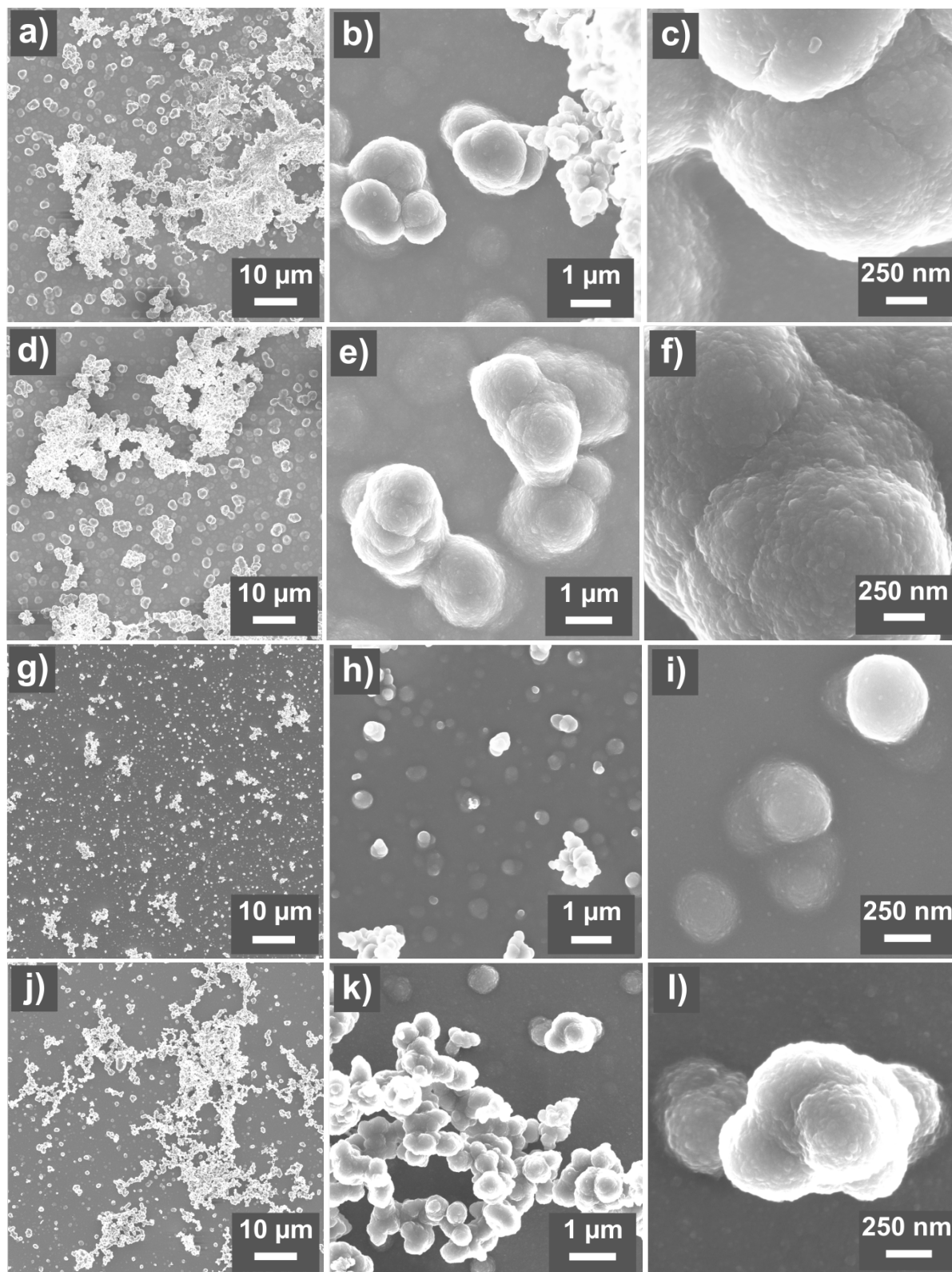


Fig. S23. SEM images at different magnifications of potentiostatically prepared films: (a–c) **p11** at 1.1 V, 60 min; (d–f) **p12** at 1.0 V, 60 min; (g–i) **p14c** at 1.0 V, 3×60 min (fresh solution every 60 min); and (j–l) **p13** at 0.9 V, 60 min. Conditions: 0.1 M Bu_4NPF_6 in CH_3CN , potentials vs. AgNO_3/Ag .

4 Electrochemical characterization of films

4.1 Cyclic voltammetry

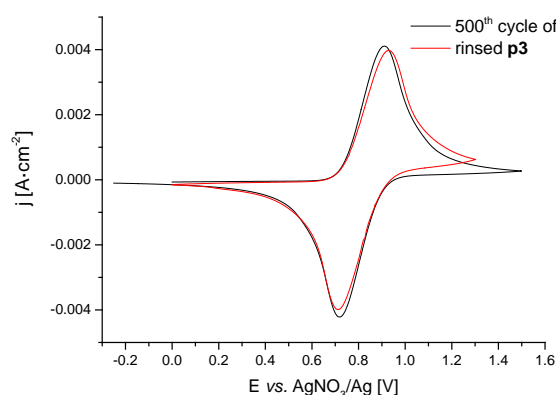


Fig. S24. Comparison of cyclic voltammetric data ($200 \text{ mV}\cdot\text{s}^{-1}$, 500 cycles; $0.1 \text{ M Bu}_4\text{NPF}_6$ in CH_3CN) exemplified for **p3** showing the 500th cycle during electropolymerization (black curve) and the rinsed film in fresh, monomer-free electrolyte solution (red curve). The small deviations may arise from kinetic contributions due to the different potential window.

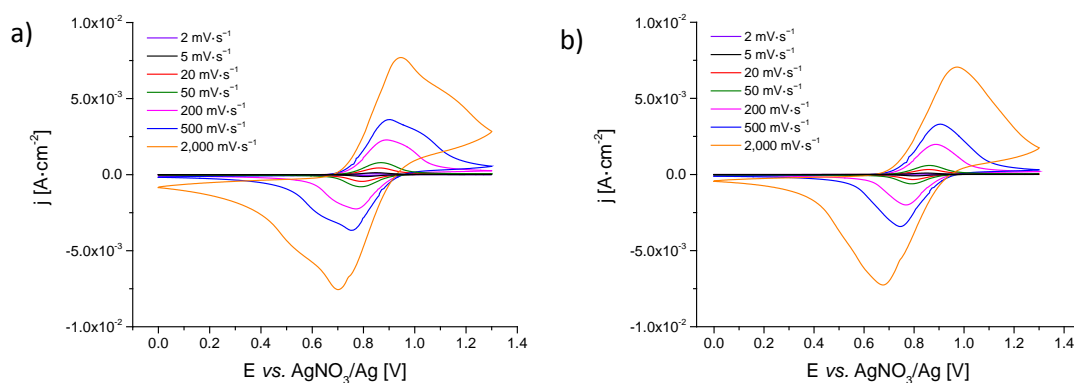


Fig. S25. CVs at different scan rates of potentiodynamically prepared films (-0.25 to $1.5 \text{ V vs. AgNO}_3/\text{Ag}$, $200 \text{ mV}\cdot\text{s}^{-1}$, 500 cycles; $0.1 \text{ M Bu}_4\text{NPF}_6$ in CH_3CN with $1\text{m}\%$ H_2O) from (a) a fresh solution (**p5a**) and (b) second attempt from the same solution (**p5b**). Measured in CH_3CN with $0.1 \text{ M Bu}_4\text{NPF}_6$.

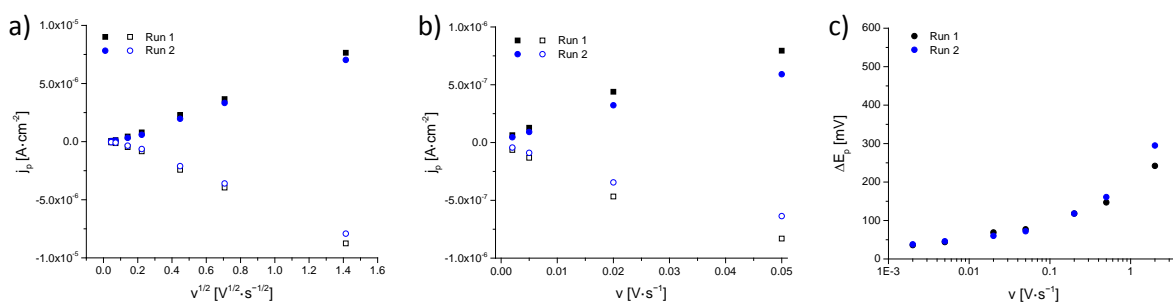


Fig. S26. Anodic and cathodic peak current densities vs. (a) $(\text{scan rate})^{1/2}$ and (b) scan rate and (c) peak potential split vs. scan rate for potentiodynamically prepared film **p5a** and **p5b** (-0.25 to $1.5 \text{ V vs. AgNO}_3/\text{Ag}$, $200 \text{ mV}\cdot\text{s}^{-1}$, 500 cycles; $0.1 \text{ M Bu}_4\text{NPF}_6$ in CH_3CN with $1\text{m}\%$ H_2O) consecutively obtained from the same solution. Measured in CH_3CN with $0.1 \text{ M Bu}_4\text{NPF}_6$.

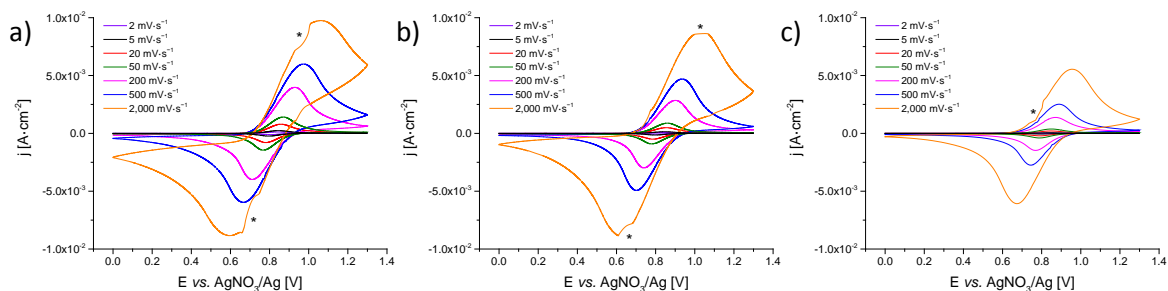


Fig. S27. CVs at different scan rates of potentiodynamically prepared films (-0.25 to 1.5 V vs. AgNO_3/Ag , $200 \text{ mV}\cdot\text{s}^{-1}$, 500 cycles; $0.1 \text{ M Bu}_4\text{NPF}_6$ in CH_3CN) consecutively obtained from the same solution (a) fresh solution (**p7a**), (b) second run (**p7b**), and (c) third attempt (**p7c**). Measured in CH_3CN with $0.1 \text{ M Bu}_4\text{NPF}_6$ (asterisks mark instrumental artifacts).

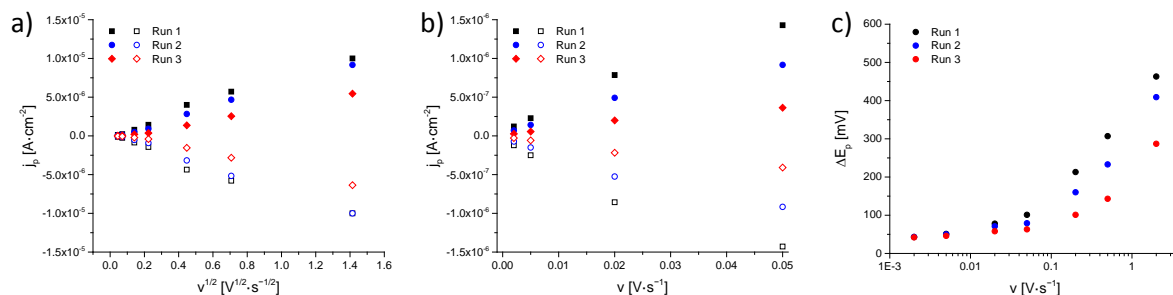


Fig. S28. Anodic and cathodic peak current densities vs. (a) $(\text{scan rate})^{1/2}$ and (b) scan rate and (c) peak potential split vs. scan rate for potentiodynamically prepared films (-0.25 to 1.5 V vs. AgNO_3/Ag , $200 \text{ mV}\cdot\text{s}^{-1}$, 500 cycles; $0.1 \text{ M Bu}_4\text{NPF}_6$ in CH_3CN) consecutively obtained from the same solution (**p7a-c**). Measured in CH_3CN with $0.1 \text{ M Bu}_4\text{NPF}_6$.

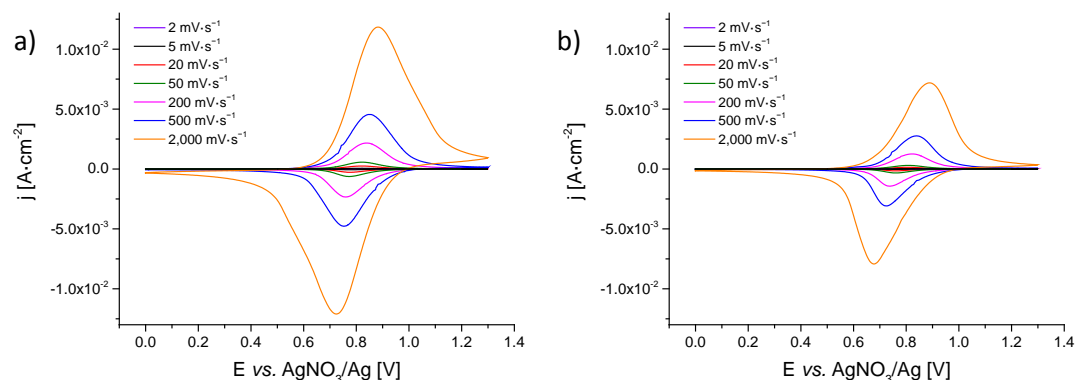


Fig. S29. CVs at different scan rates of potentiodynamically prepared films (-0.25 to 1.5 V vs. AgNO_3/Ag , $200 \text{ mV}\cdot\text{s}^{-1}$, 500 cycles; $0.1 \text{ M Bu}_4\text{NClO}_4$ in CH_3CN) from (a) a fresh solution (**p9a**) and (b) second attempt from the same solution (**p9b**). Measured in CH_3CN with $0.1 \text{ M Bu}_4\text{NClO}_4$.

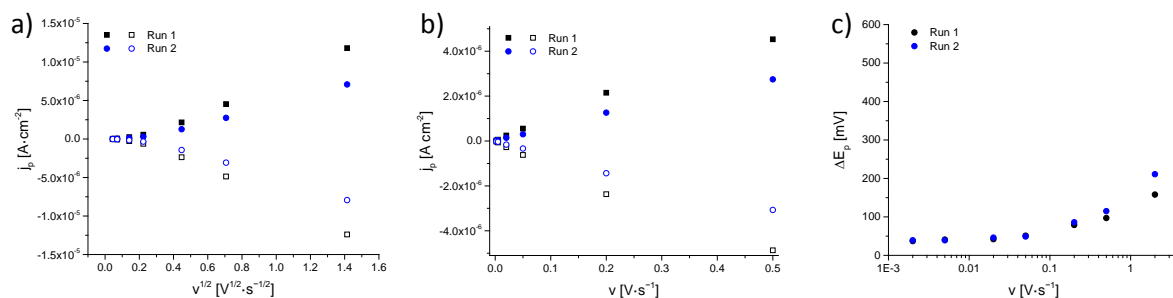


Fig. S30. Anodic and cathodic peak current densities vs. (a) $(\text{scan rate})^{1/2}$ and (b) scan rate and (c) peak potential split vs. scan rate for potentiodynamically prepared films (-0.25 to 1.5 V vs. AgNO_3/Ag , $200 \text{ mV}\cdot\text{s}^{-1}$, 500 cycles; $0.1 \text{ M Bu}_4\text{NClO}_4$ in CH_3CN) consecutively obtained from the same solution (**p9a** and **p9b**). Measured in CH_3CN with $0.1 \text{ M Bu}_4\text{NClO}_4$.

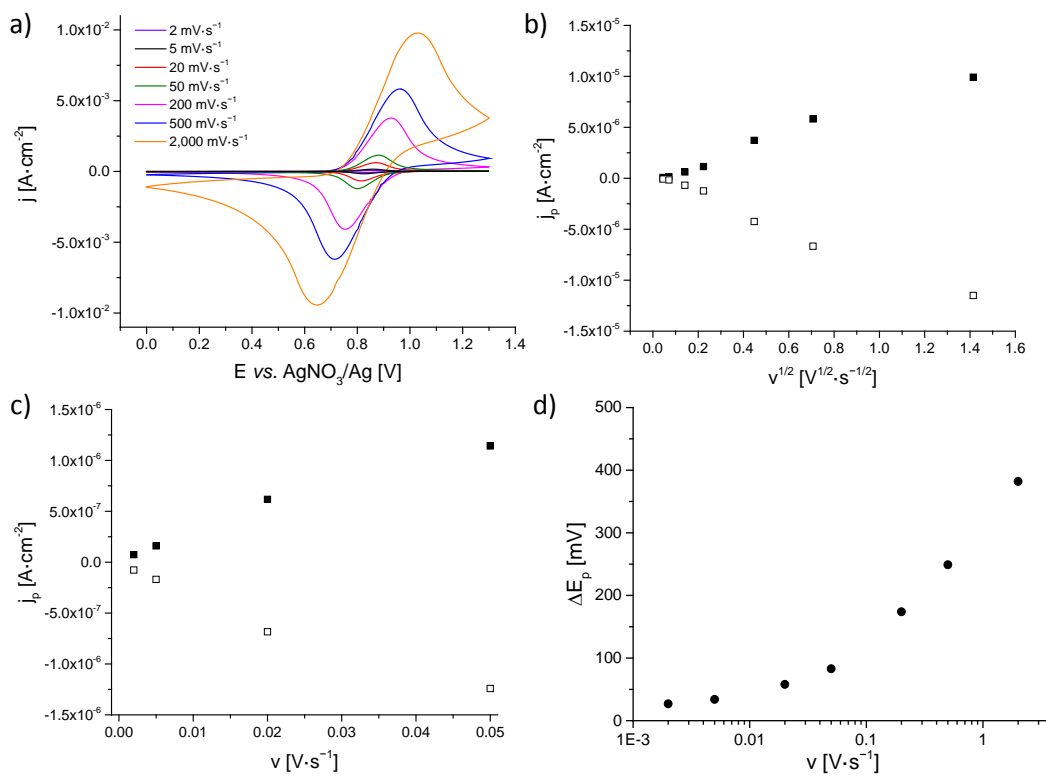


Fig. S31. (a) CVs at different scan rates, anodic and cathodic peak currents vs. (b) $(\text{scan rate})^{1/2}$ and (c) scan rate and (d) peak potential split vs. scan rate of potentiodynamically prepared film **p10** (-0.25 to 1.5 V vs. AgNO₃/Ag, 200 mV·s⁻¹, 500 cycles; 0.1 M Bu₄NPF₆ in CH₂Cl₂). Measured in CH₃CN with 0.1 M Bu₄NPF₆.

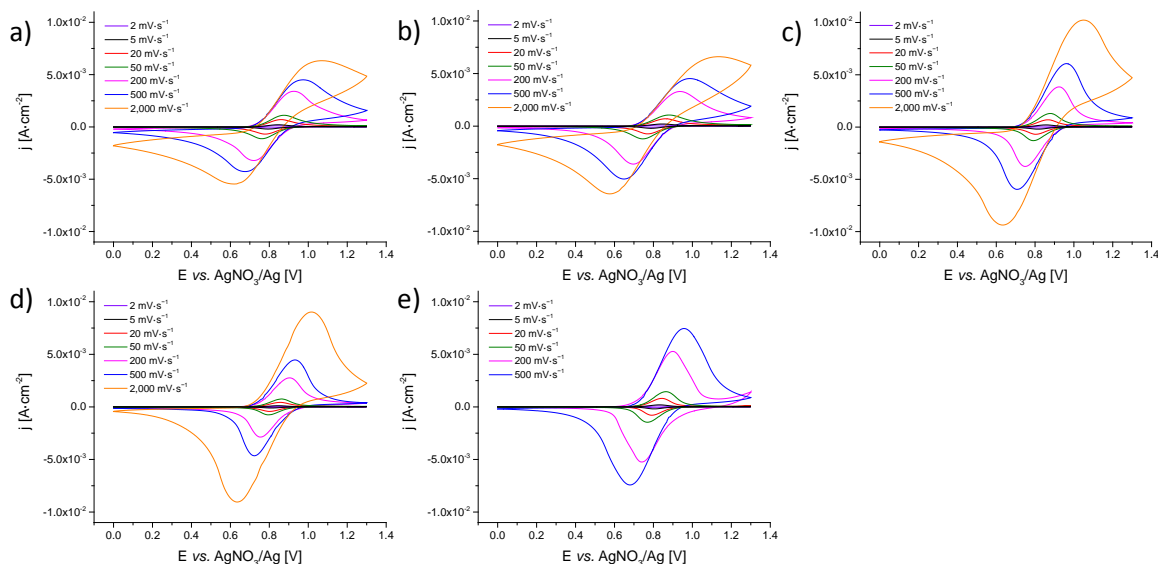


Fig. S32. CVs at different scan rates of potentiostatically prepared films: (a) **p11** at 1.1 V vs. AgNO_3/Ag , 60 min; (b) **p12** at 1.0 V, 60 min; (c) **p14c** at 1.0 V, 3×60 min (fresh solution every 60 min); (d) **p13** at 0.9 V, 60 min; (e) **p15** at 0.9 V, 240 min (0.1 M Bu_4NPF_6 in CH_3CN ; CV measured after every 5 min). Measured in CH_3CN with 0.1 M Bu_4NPF_6 .

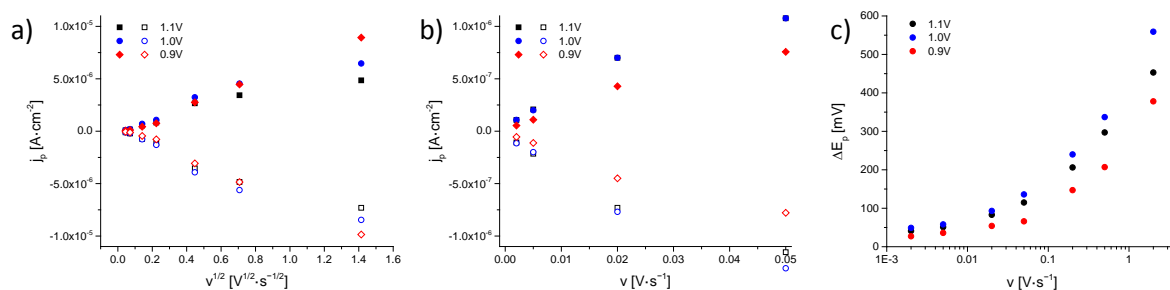


Fig. S33. Anodic and cathodic peak current densities vs. (a) $(\text{scan rate})^{1/2}$ and (b) scan rate and (c) peak potential split vs. scan rate for potentiostatically prepared films (**p11** at 1.1, **p12** at 1.0, and **p13** at 0.9 V vs. AgNO_3/Ag , 60 min; 0.1 M Bu_4NPF_6 in CH_3CN). Measured in CH_3CN with 0.1 M Bu_4NPF_6 .

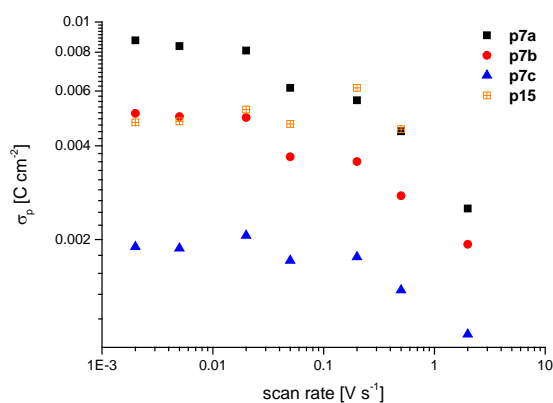


Fig. S34. Dependence of the cathodic charges with varying scan rate (2 to $2000 \text{ mV}\cdot\text{s}^{-1}$) of selected films after rinsing and re-immersion in fresh, monomer-free electrolyte (0.1 M Bu_4NPF_6 in CH_3CN). Note the deviation of the two first measurement points (at 200 and $20 \text{ mV}\cdot\text{s}^{-1}$) in the recorded series (200, 20, 500, 2, 50, 2000 and $5 \text{ mV}\cdot\text{s}^{-1}$), which is tentatively assigned to residual side reactions of reactive groups during the CV measurement.

5 Electrochemical impedance spectroscopy (EIS)

5.1 Experimental data

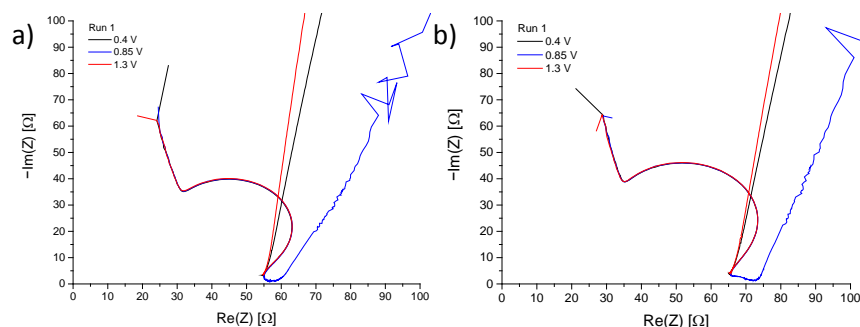


Fig. S35. EIS Nyquist plots at different dc potentials of potentiodynamically prepared films (-0.25 to 1.5 V vs. AgNO_3/Ag , $200 \text{ mV}\cdot\text{s}^{-1}$, 500 cycles; $0.1 \text{ M Bu}_4\text{NPF}_6$ in CH_3CN with $1\text{m}\%$ H_2O) from (a) a fresh solution (**p5a**) and (b) second attempt from the same solution (**p5b**). Measured in CH_3CN with $0.1 \text{ M Bu}_4\text{NPF}_6$.

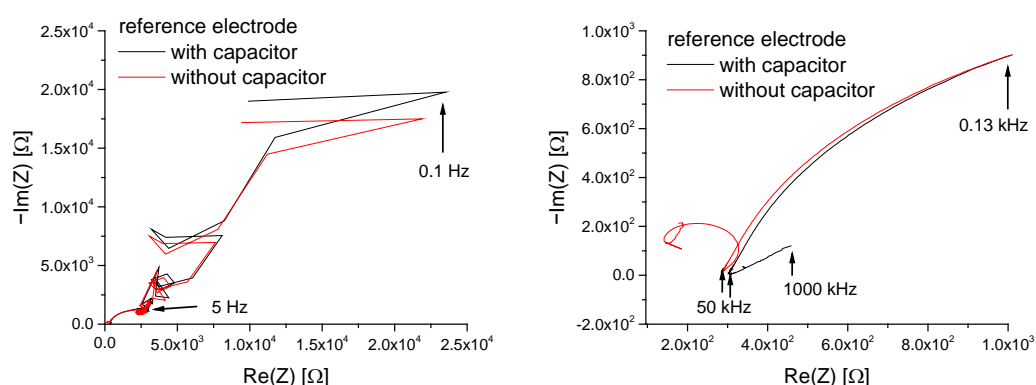


Fig. S36. EIS Nyquist plot of a potentiodynamically prepared film on glassy carbon illustrating reference electrode polarization without capacitor (red) and with capacitor (black). Note the similar curves indicating instrument artefacts at low frequencies ($< 5 \text{ Hz}$), the identical semi-circle (5 Hz to 50 kHz), and the discrepancy by reference electrode polarization ($> \sim 100 \text{ kHz}$).

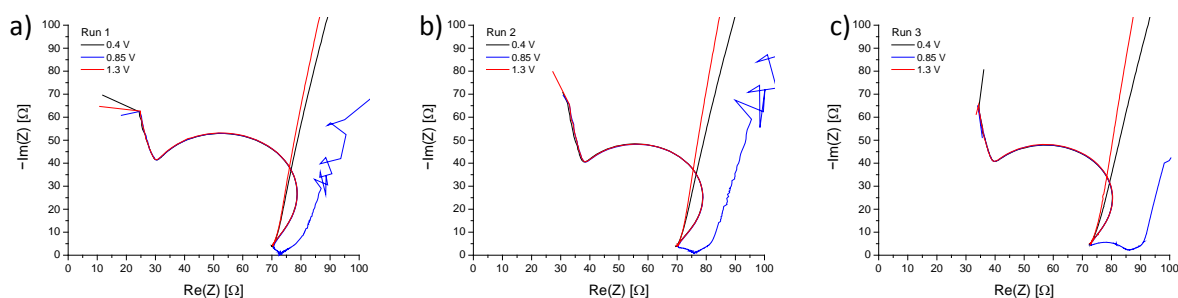


Fig. S37. EIS Nyquist plots at different dc potentials of potentiodynamically prepared films (-0.25 to 1.5 V vs. AgNO_3/Ag , $200 \text{ mV}\cdot\text{s}^{-1}$, 500 cycles; $0.1 \text{ M Bu}_4\text{NPF}_6$ in CH_3CN) consecutively obtained from the same solution: (a) first run from fresh solution (**p7a**), (b) second run onto new electrode (**p7b**), and (c) third run onto new electrode attempt (**p7c**). Measured in CH_3CN with $0.1 \text{ M Bu}_4\text{NPF}_6$.

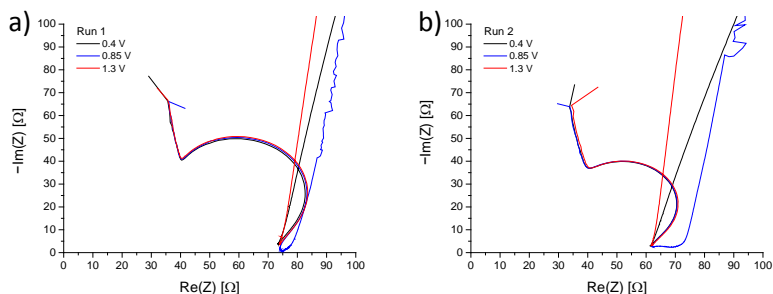


Fig. S38. EIS Nyquist plots at different dc potentials of potentiodynamically prepared films (-0.25 to 1.5 V vs. AgNO_3/Ag , $200 \text{ mV}\cdot\text{s}^{-1}$, 500 cycles; $0.1 \text{ M Bu}_4\text{NClO}_4$ in CH_3CN) from (a) a fresh solution (**p9a**) and (b) second attempt from the same solution (**p9b**). Measured in CH_3CN with $0.1 \text{ M Bu}_4\text{NClO}_4$.

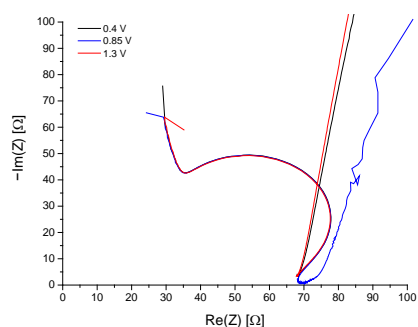


Fig. S39. EIS Nyquist plots at different dc potentials of potentiodynamically prepared film **p10** (-0.25 to 1.5 V vs. AgNO_3/Ag , $200 \text{ mV}\cdot\text{s}^{-1}$, 500 cycles; $0.1 \text{ M Bu}_4\text{NPF}_6$ in CH_2Cl_2). Measured in CH_3CN with $0.1 \text{ M Bu}_4\text{NPF}_6$.

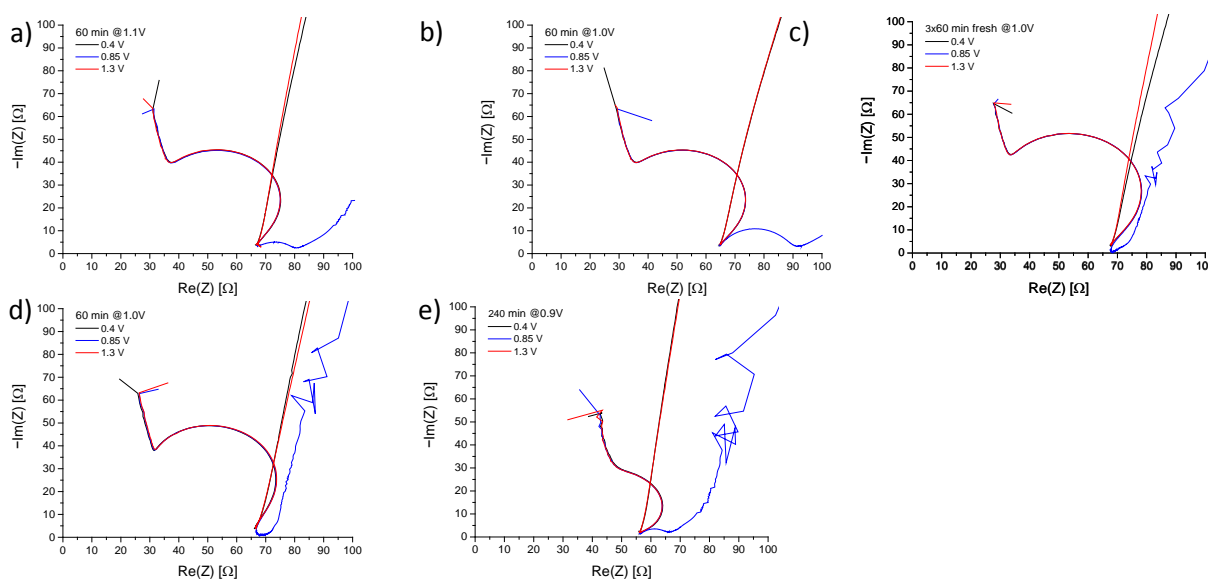


Fig. S40. EIS Nyquist plots at different dc potentials of potentiostatically prepared films ($0.1 \text{ M Bu}_4\text{NPF}_6$ in CH_3CN): (a) **p11** at 60 min at 1.1 V; (b) **p12** at 60 min at 1.0 V; (c) **p14c** at 3×60 min (immersed into fresh solution every 60 min) at 1.0 V; (d) **p13** at 60 min at 0.9 V; and (e) **p15** at 240 min at 0.9 V. Measured in CH_3CN with $0.1 \text{ M Bu}_4\text{NPF}_6$, potentials vs. AgNO_3/Ag .

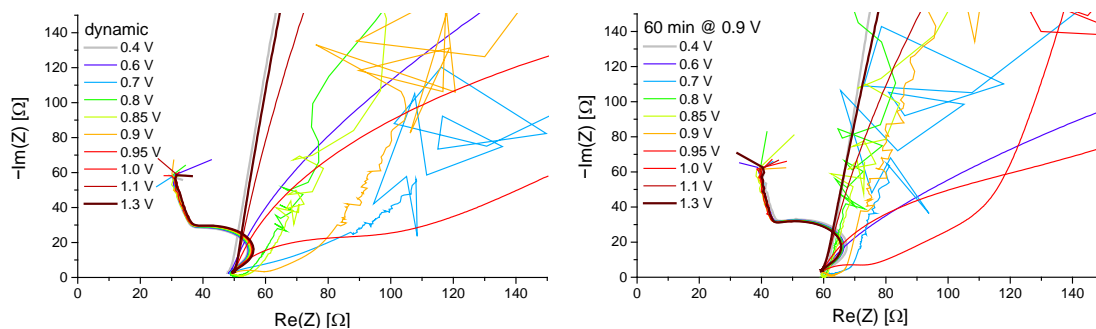


Fig. S41. Potential-dependent EIS Nyquist plots of (a) a potentiodynamically prepared film **p7a** (-0.25 to 1.5 V vs. AgNO_3/Ag , $200 \text{ mV}\cdot\text{s}^{-1}$, 500 cycles; $0.1 \text{ M Bu}_4\text{NPF}_6$ in CH_3CN) and (b) a potentiostatically prepared film **p13** (0.9 V , 60 min; $0.1 \text{ M Bu}_4\text{NPF}_6$ in CH_3CN). Measured in CH_3CN with $0.1 \text{ M Bu}_4\text{NPF}_6$.

5.2 Analysis of EIS data

The obtained impedance plots were analyzed using the EC-Lab software (Bio-Logic Science Instruments SAS). The equivalent circuit depicted in Fig. S42 was used, including the electrolyte resistance ($R_{\text{electrolyte}}$), charge transfer at a porous surface (reflected by a transmission line with pore resistance r and surface capacitance CPE q_{pore}), and charge transfer through the film (reflected by ohmic film resistance R_{bulk} and film capacitance CPE Q_{bulk}). The values obtained by respective fit procedures (using frequency data $<50 \text{ kHz}$, see Fig. S36) are summarized in Table S1, and the dependence of the rest potential is exemplified for a potentiodynamically prepared film (Table S2) and a potentiostatically prepared film (Table S3). Film conductivities σ were determined using the film resistances R_{bulk} , geometrically determined film surfaces A , and film thicknesses d estimated *via* SEM measurements (see Section 3).

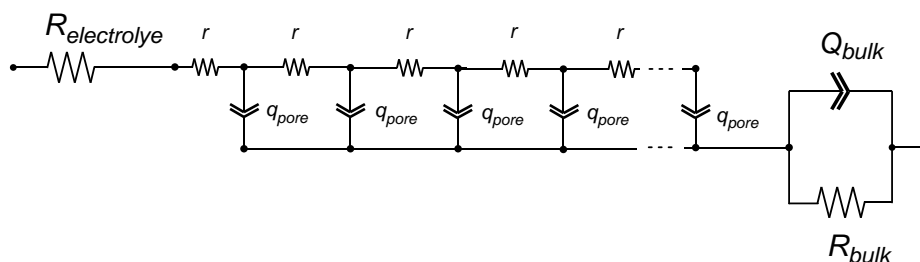


Fig. S42. Equivalent circuit used for fitting the impedance data.

Table S1. Impedance fit values for electropolymerized films at 0.85 V vs. AgNO_3/Ag .

Entry	film	$R_{\text{electrolyte}}$ [Ω]	Q_{bulk} [$\text{Fs}^{(\text{abulk}^{-1})}$]	a_{bulk}	R_{bulk} [Ω]	r_{pore} [Ω]	t_{pore} [s]	a_{pore}
1	p7a	60.4	$7.5 \cdot 10^{-7}$	0.878	11.7	19.2	0.467	0.815
2	p7b	63.6	$3.1 \cdot 10^{-5}$	0.647	11.6	17.6	0.192	0.852
3	p7v	69.0	$2.6 \cdot 10^{-5}$	0.727	16.0	16.5	0.0582	0.886
4	p9a^a	74.0 ^a	0.0243 ^a	1 ^a	0.935 ^a	10.4 ^a	0.0318 ^a	0.871 ^a
5	p9b	58.0	$2.7 \cdot 10^{-4}$	0.529	10.8	13.7	0.0205	0.898
6	p10	65.7	$5.7 \cdot 10^{-4}$	0.516	3.93	13.6	0.243	0.833
7	p5a	53.0	$7.2 \cdot 10^{-4}$	0.541	3.93	6.67	0.0284	0.703
8	p11	64.9	$4.0 \cdot 10^{-5}$	0.763	12.6	31.0	0.536	0.690
9	p12	63.0	$1.1 \cdot 10^{-5}$	0.87	23.9	24.0	0.288	0.602
10	p13	65.6	$3.8 \cdot 10^{-4}$	0.66	3.28	10.9	0.125	0.876
11	p16	55.0	$1.07 \cdot 10^{-5}$	0.668	10.4	3.56	0.0148	0.485

^a Manual fitting required, values not discussed in manuscript.

Table S2. Impedance fit values for potentiodynamically electropolymerized film **p7a** at various potentials.

Potential vs. AgNO ₃ /Ag [V]	R _{electrolyte} [Ω]	Q _{bulk} [Fs ^(a_{bulk}-1)]	a _{bulk}	R _{bulk} [Ω]	r _{pore} [Ω]	t _{pore} [s]	a _{pore}
0.40	47.0	8.02·10 ⁻⁶	0.931	6.52·10 ⁴	0.0002	3.4·10 ⁻⁶⁸	0.06
0.60	47.1	3.98·10 ⁻⁵	0.815	403	1.01	1.1·10 ⁻⁵	0.82
0.70	46.3	7.42·10 ⁻⁴	0.553	12.8	217	0.73	0.905
0.80	48.6	9.12·10 ⁻⁴	0.647	1.64	11.3	0.234	0.775
0.85	45.0	6.69·10 ⁻⁵	0.618	6.6	12.9	0.216	0.775
0.90	47.3	4.16·10 ⁻⁵	0.782	8.15	39.4	0.206	0.686
0.95	47.4	4.85·10 ⁻⁵	0.791	40.6	3·10 ⁻⁷	5·10 ⁻²⁰	0.474
1.00	46.0	3.38·10 ⁻⁵	0.811	250	2·10 ⁻⁸	2·10 ⁻¹⁸	0.635
1.10	49.1	9.31·10 ⁻⁶	0.906	8.9·10 ³	0.153	1.2·10 ⁻²⁸	8.66·10 ⁻¹⁵
1.30	49.2	7.04·10 ⁻⁶	0.93	1.66·10 ⁵	0.289	1.6·10 ⁻³⁶	4.41·10 ⁻¹²

Table S3. Impedance fit values for potentiostatically (+0.9 V) electropolymerized film **p13** at various potentials.

Potential vs. AgNO ₃ /Ag [V]	R _{electrolyte} [Ω]	Q _{bulk} [Fs ^(a_{bulk}-1)]	a _{bulk}	R _{bulk} [Ω]	r _{pore} [Ω]	t _{pore} [s]	a _{pore}
0.40	60.4	1.12·10 ⁻⁵	0.908	8.86·10 ³	0.0464	4.9·10 ⁻⁷	1
0.60	57.1	8.4·10 ⁻⁵	0.671	343	0.0397	4.9·10 ⁻⁶	1
0.70	58.1	3.01·10 ⁻⁶	1	3.37	22.4	0.0238	0.888
0.80	59.0	1.05·10 ⁻⁴	0.911	0.807	2.5	0.0342	0.897
0.85	57.9	2.11·10 ⁻⁴	0.641	2.19	2.74	0.0303	0.893
0.90	55.0	6.93·10 ⁻⁶	0.784	6.97	14.44	0.0558	0.914
0.95	57.3	1.32·10 ⁻⁵	0.869	10.6	124.6	0.111	0.879
1.00	56.0	2.06·10 ⁻⁵	0.888	65.8	3·10 ⁻⁵	5·10 ⁻¹⁵	0.552
1.10	58.4	9.99·10 ⁻⁶	0.872	3870	2·10 ⁻⁹	7.05	6.5·10 ⁻⁶
1.30	59.2	6.54·10 ⁻⁶	0.917	6.51·10 ⁴	1·10 ⁻⁹	4.64	9.35·10 ⁻⁴

Table S4 Impedance fit values for potentiostatically (+0.9 V) from CH₂Cl₂ electropolymerized film **p16** at various potentials.

Potential vs. AgNO ₃ /Ag [V]	R _{electrolyte} [Ω]	Q _{bulk} [Fs ^(a_{bulk}-1)]	a _{bulk}	R _{bulk} [Ω]	r _{pore} [Ω]	t _{pore} [s]	a _{pore}
0.40	60.3	2.92·10 ⁻⁵	0.963	1250	15.4	8.3·10 ⁻⁵	0.955
0.45	60.0	2.59·10 ⁻⁵	0.987	982	15.9	8.2·10 ⁻⁵	0.949
0.50	60.5	1.63·10 ⁻⁵	0.964	1750	14.46	9.4·10 ⁻⁵	0.949
0.55	61.2	1.26·10 ⁻⁵	0.936	1500	10.9	1.2·10 ⁻⁴	0.96
0.60	63.4	1.72·10 ⁻⁵	0.896	641	0.0307	1.8·10 ⁻⁵	0.898
0.65	61.3	7.03·10 ⁻⁵	0.754	238	2·10 ⁻⁷	4.9·10 ⁻¹⁵	0.746
0.70	61.0	2.06·10 ⁻⁴	0.758	14.7	6·10 ⁻¹²	7.6·10 ⁻²⁹	0.508
0.75	60.9	1.91·10 ⁻⁴	0.618	8.54	8·10 ⁻¹⁰	1·10 ⁻²⁴	0.478
0.80	55.0	7.17·10 ⁻⁵	0.525	12	2·10 ⁻⁵	8.5·10 ⁻²¹	0.472
0.85	55.0	1.07·10 ⁻⁵	0.668	10.4	3.56	0.0148	0.485
0.90	49.6	3.79·10 ⁻⁵	0.512	17.6	2.07	0.00153	0.483
0.95	60.3	6.95·10 ⁻⁵	0.712	10.4	8.21	0.00184	0.496
1.00	57.2	1.11·10 ⁻⁵	1	19.9	12.6	1.1·10 ⁻⁴	0.446
1.05	61.5	1.65·10 ⁻⁵	0.847	1170	0.723	2.10·10 ⁻⁵	1
1.10	61.2	1.61·10 ⁻⁵	0.915	1640	10.6	8.76·10 ⁻⁵	0.948
1.15	60.2	3.71·10 ⁻⁵	0.906	806	13.9	6.98·10 ⁻⁵	0.949
1.20	64.0	4.43·10 ⁻⁵	0.87	1980	3·10 ⁻⁶	8.34·10 ⁻¹²	0.935

6 UV-vis Characterization

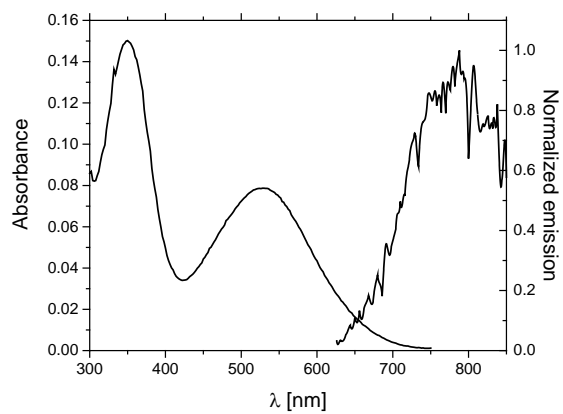


Fig. S43. Representative UV-vis absorption and emission spectra of the electropolymerized film p7a.